Title Page

Cytokine-mediated increase in endothelial-leukocyte interaction mediates brain capillary plugging during CAR T cell neurotoxicity

Lina Park,[1] Yu-Tung Tsai,[1] Hyun-Kyoung Lim,[1,2] Lila D. Faulhaber,[1] Katelyn Burleigh,[3] Eli M. Faulhaber,[1] Mahashweta Bose,[1] Andy Y. Shih,[2,4,5] Alexandre Y. Hirayama,[6,7] Cameron J. Turtle,[6,8,9] Colleen E. Annesley,[4,10] Rebecca A. Gardner,[4,10,11] Heather H. Gustafson,[3,4] Juliane Gust[1,12].

[1] Norcliffe Foundation Center for Integrative Brain Research, Seattle Children's Research Institute, Seattle, Washington, USA.

[2] Center for Developmental Biology and Regenerative Medicine, Seattle Children's Research Institute, Seattle, Washington, USA.

[3] Ben Towne Center for Childhood Cancer and Blood Disorders Research, Seattle Children's Research Institute, Seattle, Washington, USA.

[4] Department of Pediatrics, University of Washington, Seattle, Washington, USA.

[5] Department of Bioengineering, University of Washington, Seattle, Washington, USA.

[6] Fred Hutchinson Cancer Center, Seattle, Washington, USA.

[7] Division of Hematology and Oncology, Department of Medicine, University of Washington School of Medicine, Seattle, Washington, USA.

[8] Royal North Shore Hospital, St. Leonards, NSW, Australia.

[9] University of Sydney, Camperdown, NSW, Australia.

[10] Center for Clinical and Translational Research, Seattle Children's Research Institute, Seattle, Washington, USA.

[11] Department of Oncology, St. Jude Children's Research Hospital, Memphis, Tennessee, USA.

[12] Department of Neurology, University of Washington, Seattle, Washington, USA.

Correspondence to:

Juliane Gust, MD, PhD

Seattle Children's Research Institute

1900 9th Ave

Seattle, Washington, 98101, USA

Phone: 206-987-2078

Email: juliane.gust@seattlechildrens.org

Abstract

CD19-directed CAR T cells treat cancer, but also cause immune effector cell associated neurotoxicity syndrome (ICANS). Despite strong epidemiologic links between cytokine release syndrome and ICANS, it is uncertain how elevated systemic cytokines and activated immune cells cause brain dysfunction. We previously showed that leukocytes plug brain capillaries in an immunocompetent mouse model of CD19-CAR neurotoxicity. Here, we used the same model to explore how integrin activation and endothelial adhesion molecule expression contribute to capillary plugging. In vivo two-photon imaging revealed increased expression of ICAM-1 on brain capillaries, with spatially restricted VCAM-1 increases. TNF, IFN-γ, and IL-1β at concentrations equivalent to CAR T cell patient blood levels upregulated ICAM-1 and VCAM-1 in brain microendothelial cells. In mice, CAR T cells strongly upregulated VLA-4 (integrin α4β1) affinity to VCAM-1, but not affinity of LFA-1 (integrin αLβ2) to ICAM-1. Blocking integrin α4 but not integrin αL improved ICANS behavior in mice. In human CAR T cell patients, increased soluble ICAM-1 and VCAM-1 are associated with ICANS, and integrin α4 but not integrin αL is upregulated in CAR T cells after infusion. Our study highlights that cytokine-driven upregulation of endothelial-leukocyte adhesion may be sufficient to induce neurovascular dysfunction in CAR T cell patients.

Graphical Abstract

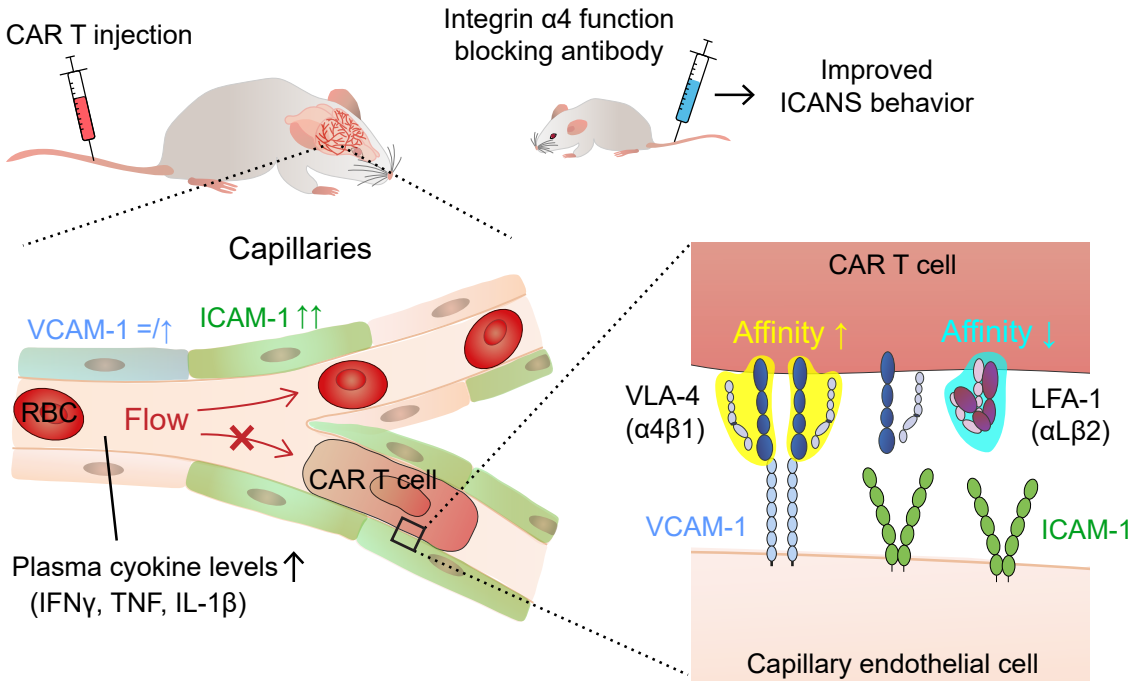

Introduction

Neurotoxicity has long been recognized as a characteristic adverse event following chimeric antigen receptor (CAR) T cell therapy for hematologic malignancies (1). The clinical syndrome has been termed immune effector cell associated neurotoxicity syndrome (ICANS) (2) based on the observation that different CAR products can cause a similar constellation of symptoms. The typical patient with ICANS will experience cytokine release syndrome (CRS) within the first week after CAR T cell infusion, followed by a decline in mental status a day or two later. Although these symptoms typically resolve without specific intervention, in some cases patients can rapidly progress to critical neurologic illness with seizures, coma, and rarely irreversible cerebral edema (1, 3).

We have previously shown in an immunocompetent mouse model of CD19-CAR T cell neurotoxicity that >10% of brain capillaries become obstructed by intravascular leukocytes in the setting of cytokine release (4). This observation was made by *in vivo* multiphoton imaging through a thinned skull window. When leukocytes flow through brain capillaries in normal conditions, they deform into an oblong shape to fit through these small channels. We hypothesized that the increased capillary stalling we observed could be caused by capillary constriction, decreased overall blood flow, and/or increased adhesion between the leukocyte and the capillary endothelium (5). Capillary diameters and systemic blood flow did not change with CAR T cell treatment (4). However, we did observe increased leukocyte-endothelial adhesion to the walls of larger vessels, particularly pial venules.

ICANS is strongly associated with systemic CRS (6). Thus, we hypothesized that high blood cytokine levels induce expression of endothelial adhesion molecules, and that activation of CAR T cells in turn activates leukocyte integrins and increases their affinity to their endothelial binding partners (7). Indeed, we now demonstrate that systemic IL-1β, TNF, and IFN-γ increase the strength of endothelial-leukocyte interactions during ICANS. This may be sufficient to induce clinically significant brain hypoperfusion due to capillary obstruction by stalled leukocytes.

Results

CAR T cell capillary plugging is associated with focal brain hypoxia

To determine the identity of the capillary plugs, we treated mice with tdTomato-coexpressing CAR T cells and imaged the cortical microvascular network by *in vivo* two-photon imaging through a chronic cranial window (Figure 1A). The circulating leukocyte pool was labeled with intravenously injected fluorescently labeled anti-CD45 antibody. CAR T cells and non-CAR T leukocytes (Figure 1, B and C) were observed to be plugging cortical capillaries. In some cases the leukocyte plugs were associated with stalled red blood cells or microthrombi (Figure 1C). The stalled red blood cells almost always appeared to be arrested behind a leukocyte plug that was obstructing blood flow, instead of being the primary cause of the obstruction. On occasion, CAR T cells could be observed crawling back and forth within the capillary, alternating with and against the direction of blood flow (Figure 1D). This indicates active interaction between the T cell and endothelium rather than a passive mechanical

process. We were not able to further specify the identity of plugging cells because other antibodies that we tested (directed against CD3, CD4, CD8, or Ly6G) led to rapid ablation of the target cells, precluding their use for stable in vivo labeling. CAR T cells were also present in the extravascular space, particularly in the meninges, but active extravasation events were observed only very rarely.

Of 154 nonflowing capillaries assessed between day 4-6 after CAR T cell infusion (n= 8 mice), 111 had visible plugs. 86% of the capillary plugs were CD45+ leukocytes. When no obstruction was visible, this was typically because nonflowing capillaries were part of an obstructed network with the obstructing object outside of the field of view. On day 4 after CAR T cell injection, the first day we observed significant capillary plugging, CAR T cells made up 72% of all CD45+ capillary plugs (range, 60-100% for individual mice). This decreased to only 13% on day 6 (range, 0-18%) (Figure 1E). This observation suggested to us that CAR T cells are first to become activated and increase their adherence to the brain endothelium, but then the immune activation spreads to other leukocyte subsets. To understand whether this shift in adherent populations is universal, we also examined the cell populations that adhere to the endothelium in larger venules of the brain border regions, namely the dura and pia. In these larger vessels, increased leukocyte adhesion occurs during CAR T cell toxicity on a similar timeline as capillary plugging, but the vessels are too large to be obstructed (4). We imaged clusters of leukocytes adherent to pial and dural venules and determined their identity (Figure 1F). Here, the proportion of CAR T cells also decreased over time, with CAR T cells representing 25% of all adherent leukocytes on day 4 (range, 11-50% for individual mice), and 12% on day 6 (range, 0-40%) (Figure 1G). Together, these results indicate

active regulation of leukocyte-brain endothelial adhesion during the peak of CAR T toxicity between day 4-6 after infusion in immunocompetent mice.

Our in vivo two-photon imaging approach was able to resolve capillary plugging to a depth of at least 150μm into the cortex (Figure 1H). To determine whether capillary plugging has detrimental effects on perfusion of the cortex or other regions that were inaccessible to our imaging approach, we performed hypoxyprobe labeling to measure the level of hypoxia in the brain tissue. CAR T cell treated mice had higher levels of hypoxyprobe labeling in the dorsal cortex compared to mice treated with mock transduced T cells (Figure 1, I-K). This corresponds to the brain region where we obtained our two-photon imaging data. There was no significant difference in hypoxyprobe labeling in other brain regions (hippocampus, thalamus, ventral cortex-striatum, and hypothalamus) between mock and CAR T treated mice. This data indicates that leukocyte plugging is associated with focal hypoxia in the cortex.

Differential regulation of ICAM-1 and VCAM-1 in brain capillaries after CAR T cell treatment

To understand how adhesion molecule expression changes in the brain microendothelium during CAR T cell treatment, we focused on expression of intercellular adhesion molecule-1 (ICAM-1) and vascular cell adhesion molecule-1 (VCAM-1), the principal cell adhesion molecules that regulate neuroinflammation (5). We have previously shown that soluble ICAM-1 and VCAM-1 increase in the blood of immunocompetent mice after treatment with CD19-CAR T cells, and that ICAM-1 but

not VCAM-1 increases in whole brain lysates of these mice (4). To better understand whether brain capillaries specifically upregulate these adhesion molecules to increase adhesion of circulating leukocytes, we first measured ICAM-1 and VCAM-1 expression in cortical capillaries by immunohistochemistry on brain sections. On day 6 after CAR T cell infusion, when capillary plugging is most severe (4), ICAM-1 was upregulated in cortical capillaries of CAR T cell treated mice (median 170% expression compared to non-CAR T controls, n=4-6 per group, P=0.0095) (Figure 2, A and B). In contrast, VCAM-1 expression varied widely between individual mice, and was overall not increased (median 76% expression compared to control, P=0.9999) (Figure 2C).

To investigate the spatial distribution of ICAM-1 and VCAM-1 expression changes, and to better understand why adhesion of leukocytes was heterogeneous across the microvascular network, we developed a method to investigate ICAM-1 and VCAM-1 expression changes *in vivo* during CAR T cell neurotoxicity. Mice implanted with chronic cranial windows were treated with CAR T cells, and immediately prior to imaging, we intravenously injected fluorescently labeled antibodies directed against ICAM-1 (Alexa 594) and VCAM-1 (FITC). On day 5 after CAR T cell infusion, ICAM-1 expression increased homogenously across capillaries (Figure 2D). VCAM-1 expression was primarily found in postcapillary venules in both mock and CAR T cell treated mice (Figure 2D). In CAR T but not mock treated mice, VCAM-1 expression extended into some of the capillaries draining into high-expressing postcapillary venules, but overall did not appear increased across the majority of the capillary network. Taken together, these results indicate that ICAM-1 expression is upregulated across the cortical capillary

network in response to CAR T cell therapy, while VCAM-1 expression only appears to increase in a spatially restricted fashion that is difficult to capture in a bulk analysis.

Cytokines induce ICAM-1 and VCAM-1 expression in human brain endothelium in vitro

CAR T cell treatment can lead to extremely high cytokine levels in the blood, and elevations of multiple blood cytokines have been associated specifically with ICANS in clinical studies (6). We have also shown similar increases in IL-6, IFN-γ, and other serum cytokines in our mouse model (4). It follows that these cytokines might increase expression of ICAM-1 and VCAM-1 in the brain microendothelium. Proinflammatory cytokines, including TNF, IL1-β and IFN-γ, are known to activate endothelial cells and upregulate adhesion molecule expression (8). However, most prior studies have used very high, supraphysiologic doses of cytokines applied *in vitro* to endothelial cells, and the brain-specific microendothelial response has not been well characterized. To determine the effect of specific ICANS-associated cytokines on the brain microendothelium, we applied a panel of cytokines to primary human brain microendothelial cell (HBMEC) monolayer cultures and measured ICAM-1 and VCAM-1 expression by flow cytometry. The range of cytokine concentrations was chosen to represent the range that has been reported in CAR T cell patients during CRS and/or ICANS (9–13), reviewed in Gust et al. (6). Healthy control blood cytokine levels were per Bender et al., Kim et al., and Yan et al. (14-16). Of the cytokines we tested, TNF, IL1-β and IFN-γ induced ICAM-1 at doses analogous to levels seen in patients (Figure 2E). VCAM-1 expression was weakly upregulated by TNF and IL1-β. The other

cytokines, including IL-6, had no effect on ICAM-1 or VCAM-1 expression (Figure 2E, Supplemental Figure S1). These results confirm that brain microendothelial cells upregulate ICAM-1 even with low levels of proinflammatory cytokine stimulation, whereas VCAM-1 responds less vigorously. This is consistent with our *in vivo* findings in mice, where a VCAM-1 response primarily occurs in microvenular endothelial cell subpopulations. These subpopulations may not be present in large numbers in cultured primary HBMECs.

CAR T cell integrins preferentially increase affinity to VCAM-1 rather than ICAM-1

The strength of leukocyte-endothelial interaction is regulated by conformational changes in integrins that occur upon leukocyte activation (7). The key integrins in neuroinflammation are VLA4 (the integrin α4β1 heterodimer) which binds VCAM-1, and LFA1 (the integrin αLβ2 heterodimer), which binds ICAM-1 (7, 17).

To measure the affinity of leukocyte integrins VLA4 and LFA1 to their endothelial binding partners, we incubated fresh whole blood from CD19-CAR T cell treated mice with fluorescently labeled ICAM-1 and VCAM-1 peptide multimers (Figure 3, A and B) and quantified multimer binding to leukocytes by flow cytometry (gating strategy shown in Supplemental Fig S2). The affinity of T cell LFA-1 to ICAM-1 was not higher in CAR T cell treated mice compared to mock controls on days 5, 12, or 19 after CAR T cell infusion (Figure 3C). In fact, CAR T cells had lower ICAM-1 affinity than native, CAR-negative circulating T cells on day 5 and 12 after CAR T cell infusion (Figure 3C, Supplemental Figure S3). Although cell surface expression of integrin αL (LFA-1) in T cells was higher in CAR T cell treated mice compared to mock controls (Figure 3D), its

expression actually dropped in CAR T cells over time, whereas native T cells in the same mice saw a transient increase (Figure 3D, Supplemental Figure S3). The pattern of decreasing LFA-1 expression and affinity over time means that the LFA-1/ICAM-1 interaction likely only makes a minor contribution to the increase in leukocyte-endothelial adhesion during CAR T toxicity.

In contrast, T cell expression of integrin α4 and the affinity of VLA-4 to VCAM-1 increased dramatically after CAR T cell infusion (Figure 3, E and F). Both CAR T cells and native T cells showed the same behavior, but it was much more pronounced in CAR T cells. Both subsets of T cells showed a sharp increase by day 5, followed by a decline without return to baseline by day 12 and 19 (Supplemental Figure S3). This was primarily driven by CD8+ CAR T cells (Supplemental Figure S4). In contrast, among native T cells CD4+ T cells had higher ICAM-1 and VCAM-1 affinity, even though CD8+ T cells more strongly upregulated integrin expression (Supplemental Figure S4). Expression levels of integrin α4 (VLA-4) showed the same temporal pattern of rise and fall which was most pronounced in the CD8+ subset for both native and CAR+ T cells (Supplemental Figure S4). Taken together, these results indicate that CAR T cell binding to VCAM-1 but not ICAM-1 is activated when the CAR T cells encounter antigen in vivo. The concomitant increase in VCAM-1 affinity of native T cells may be mediated by cell-cell signaling, and/or by the proinflammatory cytokine/chemokine milieu (7).

We also measured the affinity of LFA-1 and VLA-4, as well as the surface expression of integrins αL and α4, on Ly6G+ neutrophils and CD11b+/Ly6G- myeloid cells. In both cell populations, we observed no significant changes in integrin affinity between CAR T treated mice and mock controls (Supplemental Figure S5). Similarly, surface expression

of integrins αL and α4 did not change, with the exception of a slight increase in VLA4 expression on CD11b+/Ly6G- myeloid cells in CAR T mice on day 5 (Supplemental Figure S5). These results show that, among leukocytes, integrin activation and expression are not significantly altered in myeloid cells, but rather in the T cells, particularly the CAR T cells.

VLA4 blockade improves locomotion in CAR T mouse model

Our data so far suggests that the interaction of VLA-4 with VCAM-1 is strongly modulated during CAR T cell treatment, and its dynamics align with the timing of CAR T cell neurotoxicity, with a peak on day 5 after CAR T cell infusion. We reasoned that blockade of this interaction may decrease clinical CAR T cell neurotoxicity. We have previously shown that locomotion activity is severely impaired in mice experiencing neurotoxicity after CD19-CAR T cell treatment (4). We used the same testing paradigm and treated mice with 2mg/kg per dose of antibodies directed against integrin α4 or integrin αL on days 1, 3, and 5 after CAR T cell infusion. Mice receiving integrin α4 blockade moved a median of 133% the distance compared to mice receiving isotype control antibody (P=0.0234) (Figure 3G), whereas no such effect was seen with integrin αL blockade (99% distance moved compared to isotype control, P=0.5781) (Figure 3H).

In CD19-CAR T cell patients, increases in soluble ICAM-1 and VCAM-1 are associated with ICANS and correlate with serum cytokine levels

Next, we sought to determine if ICAM-1 and/or VCAM-1 levels are also associated with ICANS in human CAR T cell patients. It would stand to reason that the increased cytokine levels that are seen after CD19-CAR T cell infusion (6) can induce ICAM-1 and VCAM-1 expression in the endothelium, similar to what we found in vitro in brain microendothelial cells and in the ICANS mouse model. We measured the concentration of soluble ICAM-1 and VCAM-1 in the plasma of CD19-CAR T cell treated patients at baseline (day 1 after CAR cell infusion) and on day 7 after CAR T cell infusion in adult (n=48 patients) (18) and pediatric cohorts (n=61 patients) (19). In both groups, the ratio of day 7 to day 1 soluble ICAM-1 and VCAM-1 levels was higher in patients with ICANS compared to patients without ICANS (Figure 4A, Supplemental Table 1). Baseline ICAM-1 and VCAM-1 levels were not different between patients with or without subsequent ICANS (Supplemental Table 1). We next tested whether the cytokines that induced ICAM-1 and VCAM-1 in vitro also correlated with in vivo induction in patients. Indeed, higher serum levels of IFN-γ and TNF on day 7 after CAR T cell infusion were associated with greater rises in soluble ICAM-1 and VCAM-1 (Figure 4, B and C). Although IL-6 did not induce either adhesion molecule in vitro, patients with serum IL-6 levels of >100pg/mL also had a significantly greater rise in soluble ICAM-1. This data must be interpreted with the caveat that patients with high IL-6 levels also typically have high IFN-γ and TNF levels. In addition, the measurements of soluble ICAM-1 and VCAM-1 reflect only the systemic circulating molecules and are not specific to the brain endothelium. Nonetheless, this data is consistent with a mechanism of toxicity where increased ICAM-1 and/or VCAM-1 expression in the brain endothelium is induced by circulating proinflammatory cytokines.

CAR T cells upregulate integrin α4 expression in human CD19-CAR T cell patients

Our mouse data indicated that the interaction of VLA-4 with VCAM-1 is exquisitely regulated by CAR T cells and native T cells. To determine if this is the case in human CAR T cell patients, we reanalyzed a published single-cell RNA sequencing dataset from patients treated with commercially available CAR T products (20). We compared pseudobulk gene expression levels of integrin α4 (ITGA4) and integrin αL (ITGAL) between CAR T cells in the infusion product and sorted CAR T cells from day 7 PBMCs (n=12 patients), and between circulating non-CAR T cells at baseline and day 7 (n=11 patients). Similar to what was seen in mouse CAR T cells, ITGA4 expression rose substantially in CAR T cells after they were infused (P=0.0002) while ITGAL expression did not change (P=0.2874) (Figure 4D). Native T cells did not see a concomitant change in either integrin's expression level between baseline and day 7 after CAR T cell infusion (Figure 4D). This is unlike in the mouse model, where both increased. This difference could be due to the fact that the mice were healthy prior to CAR T cell treatment, whereas the patients may have had previously activated circulating T cells due to multiple prior therapies, lymphodepleting chemotherapy, and/or infections.

Discussion

Brain capillary plugging by leukocytes occurs during CAR T cell toxicity, as we have previously shown in our immunocompetent CD19-CAR mouse model. The associated brain tissue hypoxia may be sufficient to cause transient cognitive dysfunction, which

would be expected to resolve once the plugging is cleared. This is consistent with the natural history of ICANS in human patients, where symptoms typically reach their maximum within days after onset, and then gradually resolve (3, 9). If plugging were to become more severe, it could lead to overt tissue injury and even cerebral edema if brain perfusion is globally impaired.

The risk of ICANS is strongly associated with preceding CRS, and ICANS typically develops soon after the peak of CRS (6). This observation led us to the overarching hypothesis that capillary plugging is induced by cytokine release with concomitant endothelial activation and leukocyte activation during the acute inflammatory phase of CAR T cell therapy. Such a mechanism would be independent of any off-tumor on-target activity of the CAR T cells, and would be consistent with ICANS as an overarching syndrome of neurotoxicity that could occur with any cytokine-activating immunotherapy.

Our findings in this study largely support this hypothesis. We show that the brain endothelium can be activated by relatively modest increases in IL1-β, IFN-γ and TNF, reflective of blood levels that are typically found in CAR T cell patients. Circulating CAR T cells and native T cells increase their interaction with endothelial adhesion molecules by upregulating integrin affinity. We also found that there is nuance to the details of these interactions, which may provide a hint as to why ICANS is such a brain-specific syndrome. If endothelial-leukocyte adhesion was broadly upregulated throughout the body, one would expect predictable organ dysfunction in other organs such as the kidneys. However, this has not been observed.

The first nuance is that while ICAM-1 is globally upregulated in brain capillaries after CAR T cell treatment, the regulation of VCAM-1 expression appears to be restricted to

specific locations. These niches may contain specialized pro-inflammatory endothelial cell populations, termed “reactive endothelial venules” by a recent study of single cell gene expression in healthy and inflamed brain endothelium (21). Better understanding of such specialized endothelial populations will require spatial gene expression analysis and live imaging studies that can capture the dynamic nature of these niches, and determine whether spatially restricted VCAM-1 upregulation is sufficient to induce capillary plugging. An alternative explanation would be that basal levels of VCAM-1 expression are sufficient to induce capillary plugging as long as the VLA-4 integrin’s affinity increases sufficiently. This leads to the second complexity that modifies our basic hypothesis. Our current data suggest that even though ICAM-1 is globally upregulated in brain capillaries, it does not play a primary role in leukocyte capillary plugging, since the affinity of the cognate integrins was not increased in circulating T cells, and blocking the ICAM-1/LFA1 interaction did not lead to clinical improvement in CAR T treated mice. CAR T cells actually downregulated their affinity to ICAM-1 after infusion into the body. In contrast, there was a strong increase in CAR T cells’ affinity to VCAM-1. Improvement in neurotoxicity behavior measures after blockade of the VLA-4/VCAM-1 interaction suggests that this interaction, and not integrin LFA-1/ICAM-1, is primarily responsible for mediating clinical toxicity. Furthermore, we show that patients manifest a similar pattern of increased systemic VCAM-1 and ICAM-1 expression while their CAR T cells upregulate only ITGA4 (part of VLA-4) but not ITGAL (part of LFA-1) after infusion into the body. Of course, these integrin expression levels do not necessarily predict the integrin’s affinity/avidity to its target. To truly understand the contribution of the ICAM-1/LFA-1 vs the VCAM-1/VLA1-1 axis in human patients, future studies should

measure integrin affinity/avidity in patient T cells and other circulating leukocytes. We found that this needs to be measured on freshly isolated cells, as cryopreservation altered the integrin activation state.

The function of the ICAM-1/LFA-1 and VCAM-1/VLA-4 axes extends beyond the leukocyte-endothelial interaction. They are also important for cell-cell signaling in the immune system, immune synapse formation, and immune cell trafficking in tissues (7). Thus, other potential mechanisms of CAR toxicity are also consistent with our data, such as dysfunctional activation of the myeloid compartment (22) or direct tissue invasion. Importantly though, our data suggests that increased endothelial and/or T cell activation and subsequent capillary plugging could be sufficient to induce transient neurotoxicity due to hypoperfusion, accompanied by more permanent tissue injury in severe cases. Similar mechanisms may contribute to brain injury during sepsis, seizures, and neurodegenerative disorders (23–25).

If capillary plugging is indeed responsible for at least aspects of neurotoxicity, what are the therapeutic or preventive options? Blockade of ICAM-1 or integrin α4 has been previously tested in patients with ischemic stroke, after mouse studies suggested that decreasing leukocyte recruitment to ischemic vasculature may improve outcomes. This approach has been all but abandoned after high quality clinical trials showed either negative or even adverse outcomes (26). Use of IL-1β blockade to prevent ICANS has been supported by a mouse study (27), which however did not investigate the possible mechanism of injury that might be mediated by IL-1β. Nonetheless, IL-1β blockade with anakinra has become a mainstay of ICANS treatment, despite a paucity of data reporting IL-1β levels in the blood or CSF of CAR T patients. Clinical studies are in

progress to measure whether IL-1β blockade can decrease the incidence or severity of ICANS. Finally, engineering CAR T cells with reduced or deleted integrin expression is feasible and may reduce neurotoxicity while preserving antitumor activity (28).

Methods

Sex as a biological variable

Male and female mice were used in equal numbers, and sexes were randomly assigned to experiments. We have previously shown that there is no sex difference in CAR T neurotoxicity scores in our model (4).

Animals

5-10 week old wild-type BALB/c mice were used for all experiments. Mice were obtained from Jackson Labs (Bar Harbor, ME) and housed in specific pathogen free facilities. No experimental animals were excluded from analysis.

CAR T cell generation

The CD19-directed CAR consists of an anti-murine-CD19 single chain variable fragment (scFv) derived from the 1D3 hybridoma (29), a CD28 transmembrane domain and murine intracellular 4-1BB and CD3z costimulatory domains. It is followed by a T2A

sequence and Thy1.1 or tdTomato as a transduction marker. The construct was cloned into a MMLV backbone, and gammaretrovirus was produced by transient calcium phosphate transfection of a Phoenix-ECO producer line (ATCC). CAR T cells were generated per published protocol (30). Briefly, T cells were collected by mechanically dissociating spleens and lymph nodes of wild type BALB/c mice, followed by MACS selection with CD90.2 beads (Miltenyi Biotec). T cells were then stimulated with CD3/CD28 Dynabeads (ThermoFisher) (days 1-4), murine IL-2 (Peprotech) (days 1-3) and murine IL-15 (Peprotech) (day 4) in RPMI supplemented with 10% fetal bovine serum, penicillin/streptomycin, β-mercaptoethanol, and sodium pyruvate. On days 2 and 3, cells were spinoculated with viral supernatant at 2000xg for 1 hour on retronectin (Takara) coated plates. Transduction efficiency was verified by flow cytometry for Thy1.1. Mock transduced T cells underwent the same transduction protocol, while replacing the viral supernatant with media during the spinoculation step.

CAR T cell treatment

To reduce rejection of CAR T cells, mice received lymphodepleting chemotherapy with 250mg/kg cyclophosphamide via a single i.p. injection (Day -1). 24h later (Day 0), 5-10 x 10^6 CAR T cells or mock transduced T cells per animal were infused via the lateral tail vein. Mice were monitored with daily weight and temperature measurements, and both controls and CAR T treated animals received daily subcutaneous normal saline boluses (20mL/kg). Blood for analysis was collected via chin bleed, retro-orbital puncture under sedation, or post-euthanasia.

Cranial window preparation and anesthesia

We created polished and reinforced thinned-skull windows or chronic cranial windows over the somatosensory cortex as previously described (31,32). Briefly, anesthesia was induced with 4% isoflurane and additional pain control provided with buprenorphine. Mice were maintained at 1-2% isoflurane for surgery. After removing the skin, a custom head mount was attached using dental cement. For thinned-skull windows, the skull was thinned to translucency with a handheld drill and a 4mm coverslip was mounted on top of the area with cryanoacrylate instant adhesive. Imaging was started 1 day after the surgery. For chronic windows, the skull was removed, keeping the dura intact, and a plug fashioned of a 3mm and 4mm coverslip glued together with cryanoacrylate adhesive was mounted into the skull defect. Mice were allowed to recover for 2-3 weeks prior to imaging. During imaging, mice were anesthetized with 1.5% isoflurane and mounted in a custom head holder.

In vivo two photon imaging

Imaging was performed on a Bruker Investigator microscope with Prairie View imaging software, coupled to a Spectra-Physics InSight X3 tunable laser (680-1300nm). Green, red, and far red fluorescence emission was collected through 525/70nm, 595/50nm, and 660/40 bandpass filters, respectively. Images were collected using a 20X (1.0 NA) water-immersion objective (Olympus; XLUMPLFLN).

All antibodies and intravascular tracers were delivered by injection into the retro-orbital sinus. The blood plasma was labeled with 2mDa dextran conjugated to either FITC or Alexa 680 (5% in PBS, 20 µl once). The following monoclonal antibodies conjugated to either FITC, Alexa 488, or Alexa 568 were injected and allowed to equilibrate for at least 15 minutes prior to imaging: anti-CD45.2 (clone 104, Biolegend; 0.4mg/kg per dose), anti-ICAM-1 (clone YN1/1.7.4, Biolegend, Cat. 116102, 1mg/kg per dose), and anti-VCAM-1 (clone 429, Biolegend, Cat. 105705, 1mg/kg/dose).

Immunohistochemistry

Mice were killed by CO_2 inhalation and perfused transcardially with PBS followed by 4% paraformaldehyde and brains were dissected out. 40-50µm thick floating brain sections were incubated in blocking solution (10% donkey serum+0.1% Triton X-100 in PBS) for 1 h, then at 4°C overnight with primary antibodies directed against ICAM-1 (clone YN1/1.7.4, Biolegend, 1:100) or VCAM-1 (clone 429, Biolegend, 1:100) and laminin (rabbit polyclonal, Novus Biologicals Cat. NB300-144, 1:50) in 1% donkey serum+0.1% Triton X-100 in PBS, washed in PBS, incubated with secondary antibodies for 2h at room temperature, counterstained with DAPI and mounted in FluoromountG (Southern Biotech). Stained sections were imaged with a confocal microscope at 20X and Z-projected as a maximum intensity projection. CAR T and control mice were always processed in parallel by a scientist who was blinded to treatment conditions.

To measure expression of ICAM-1 and VCAM-1 in capillaries, regions of interest (ROIs) were defined by manually tracing each capillary segment in the laminin channel, and

measuring the brightness of the ROI in the ICAM-1 or VCAM-1 channel. Background brightness was measured by copying each ROI to an adjacent area without a vessel and again measuring the brightness of the ICAM-1 or VCAM-1 channel. Two 466x466 μm images of somatosensory cortex were analyzed per mouse, the average brightness per pixel across all capillaries (arbitrary units) was calculated across both images, and normalized by dividing the brightness value of CAR T mice by that of controls within the same experiment.

Human brain microvascular endothelial cell culture

Primary human brain microvascular endothelial cells (HBMECs) were obtained from ScienCell Research Laboratories (Cat. 1000) and cultured in flasks coated with 2% gelatin (Sigma). HBMECs from passages 3-5 were used for experiments. They were maintained in microvascular endothelial cell growth medium (Cat. CC-3202, Lonza) that includes 5% fetal bovine serum (FBS), hydrocortisone, human fibroblast growth factor-beta (hFGF-β), vascular endothelial growth factor (VEGF), R3-insulin-like growth factor-1 (R3-IGF-1), ascorbic acid, human epidermal growth factor (hEGF), and gentamicin sulfate-amphotericin (GA-1000). Cells were incubated at 37˚C with 5% CO2 and media replaced every 2 days.

Cytokine Treatment of HBMECs

Recombinant human tumor necrosis factor (TNF), interferon-γ (IFN-γ), interleukin-2 (IL-2), interleukin-4 (IL-4), interleukin-6 (IL-6), interleukin-8 (IL-8), interleukin-10 (IL-10), interleukin-15 (IL-15), granulocyte-macrophage colony-stimulating factor (GM-CSF),

and C-X-C motif chemokine ligand 10 (CXCL-10) were obtained from Peprotech and diluted in complete microvascular endothelial cell growth medium (Cat. CC-3202, Lonza) to reach final concentrations of 10 pg/ml, 100 pg/ml, and 1000 pg/ml. Recombinant human interleukin-1β (IL-1β, Peprotech) was diluted in complete growth medium to reach final concentrations of 0.5 pg/ml,1pg/ml, 2.5 pg/ml, 5 pg/ml, 10 pg/ml, and 100 pg/ml. HBMECs were cultured in 2% gelatin coated 24-well plates to 70-80% confluency and then treated with 500 µL of media containing one cytokine at various concentrations for 24 hours. Treatments were given to duplicate wells.

Cytokine-treated HBMECs were lifted from 24 well plates with TrypLE (ThermoFisher Scientific), and 50,000 cells per well were placed into 96 well plates. Cells were first stained with Live/Dead fixable far red dead cell stain (Cat. L34973, ThermoFisher Scientific) at room temperature and then stained with anti-human VCAM-1 (=CD106, clone STA, Cat. 305806, Biolegend) and anti-human ICAM-1 (=CD54, clone HA58, Cat. 353108, Biolegend) antibodies for 15 minutes on ice in the dark. Flow cytometry analysis was performed on a Novocyte flow cytometer where 10,000 cells were acquired and single cells were identified using forward scatter height versus area. Median fluorescence intensity of ICAM-1 and VCAM-1 was used for analysis.

Production of Mouse ICAM-1 and VCAM-1 multimers

Soluble fluorescent ICAM-1 and VCAM-1 multimers were produced by following a protocol adapted from Dimitrov et al (33). We incubated 200 µg/ml recombinant mouse ICAM-1-Fc chimera protein (Cat. 553006, Biolegend) or 200 µg/ml recombinant mouse

VCAM-1-Fc chimera protein (Cat. 643-VM-050, R&D Systems) with polyclonal anti-human Fc-PE F(ab')2 fragments (Cat. 109-116-170, Jackson Immuno Research) diluted 3.41x to final working volume with PBS. The multimer mixture was incubated at 4°C for 18 hours on a rocking shaker. As an example, in order to produce 100µl of ICAM-1 multimers, we mixed 20µg of ICAM-1-Fc with 29.3µl Fc-PE F(ab′)2 antibody (3.41x dilution) and diluted the mixture to 100µl final volume with PBS.

LFA-1 and VLA-4 affinity and quantification assay

We obtained whole blood samples from mice across all treatment groups (saline control, cyclophosphamide only, mock transduced T cell treated, CAR T cell treated) via chin bleed on Days -1, 5, 12, and 19 post treatment. Blood samples were processed within 1 hour after collection.

To measure the quantity and activation of integrins LFA-1 and VLA-4 on the surfaces of various leukocytes, fresh blood samples were diluted 1:1 with PBS and then transferred into a 96-well U-bottom plate at 20µl per well. After Fc blocking with anti-mouse CD16/32 (Cat. 101319, Biolegend) for 5 min, blood samples were stained with the following immunophenotyping antibodies: CD45.2 (Clone 104, Cat. 109832, Biolegend), CD3 (Clone 17A2, Cat. 100216, Biolegend), CD19 (Clone 6D5, Cat. 115530, Biolegend), CD11b (Clone M1/70, Cat. 101212, Biolegend), Ly6G (Clone 1A8, Cat. 127616, Biolegend), CD90.1 (Clone OX-7, Cat. 202503, Biolegend), CD8a (Clone 53-6.7, Cat. 100744, Biolegend), and Live/Dead Aqua (Cat. L34965, Thermo Fisher). CD11a (Clone M17/4, Cat. 101107) and CD49d (Clone PS/2, Cat. 1520-09L, Southern

Biotech) were used to detect surface integrins LFA-1 and VLA-4, respectively, while ICAM-1 and VCAM-1 multimers were used to specifically bind to activated integrins.

Samples were stained for 15 min then were fixed and lysed for erythrocytes with fix/lyse buffer (Cat. 00-5333-54, Thermo Fisher) for 10 min. Cells were washed with autoMACS buffer (Cat. 130-091-221, Miltenyi Biotec) twice before running flow cytometry.

In vivo integrin blockade behavioral test

Integrin αL function blocking antibody (Clone M17/2, Cat. BE0006, InVivoMAb), integrin α4 function blocking antibody (Clone PS/2, Cat. BE0071, InVivoMAb), or isotype control (clone LTF-2, Cat. BE0090, InVivoMAb) were retro-orbitally injected at a dose of 2mg/kg under isoflurane anesthesia on Days 1, 3, and 5 post treatment.

Mice were subjected to open field testing on Day 6 where they were introduced into a clean 20cm x 20cm x 20cm testing chamber. Video was acquired with a tracking camera above the chamber and analyzed with Noldus software. After a 5 minute acclimation period, 10 minutes of activity tracking were performed, and time spent in the center 50% of the arena and total distance traveled were measured. For statistical analysis, the distance traveled was expressed as a percentage of the total distance traveled by the cage mate control that received isotype antibody.

Human samples and analysis

Deidentified samples were obtained from patients with acute lymphoblastic leukemia who received CD19-directed CAR T cells as part of clinical trials at Seattle Children's (NCT02028455) (19) or Fred Hutch Cancer Center (NCT01865617) (34). To measure soluble VCAM-1 and soluble ICAM-1, the VPLEX Vascular Injury Panel II (Cat. K151198D-2, Meso Scale Diagnostics) was run and analyzed according to manufacturer's instructions with a 1:10,000 sample dilution. Pooled healthy serum with spiked-in standard was used on all plates as the inter-plate control; all assays used in the analysis had interplate control coefficient of variation (CV) of 3-14%. Serum cytokines were measured using Milliplex (Millipore) or Meso Scale Discovery (Meso Scale Diagnostics) assays per the manufacturers' instructions.

Single-cell data analysis

Single cell gene expression data from patients treated with commercial CD19-directed CAR T cells (GEO accession GSE197268) (20) was queried for gene expression levels of ITGA4 (integrin α4) and ITGAL (integrin αL) in CAR T cells and native T cells. Patients in the dataset were included if they had a complete response to CAR T cells, and single cell sequencing data was available for either both the infusion product and sorted CAR T cells on day 7 post infusion (Patients 7, 8, 10, 11, 15, and 19 received axicabtagene ciloleucel; patients 22, 26, 27, 29, 30, and 32 received tisagenlecleucel), and/or paired PBMC samples from baseline and day 7 (Patients 6, 8, 10, 11, 12, 13, 15 received axicabtagene ciloleucel; patients 19, 21, 22, and 30 received tisagenlecleucel). Each sample was individually clustered in Seurat using a standard single cell workflow.

Cells were filtered for less than 15% mitochondrial RNA transcripts and a minimum of 200 genes. Data was log normalized for each cell as ln(1+10^4*unique molecular identifier (UMI) count for the gene of interest/total UMI count for the cell). For every sample, all T cell clusters were included in pseudobulk gene expression analysis. For each gene of interest, the summed number of log normalized UMIs in the population of interest was divided by the number of cells in the population to obtain a mean expression level per cell.

Statistical analysis

All analyses were performed blinded to the treatment group. Where appropriate, normality tests were performed prior to statistical tests. When normality was met, parametric analysis (t-test, one-way ANOVA with Holm–Sidak post-test to account for multiple comparisons, Pearson's correlation) was performed and means were reported. Otherwise, nonparametric analyses (Mann–Whitney test, Spearman correlation) were performed and the median values were reported. The specific test used is indicated in the text and/or figure legends. Differences were considered statistically significant at the 95% confidence level. All statistical analyses were performed in GraphPad Prism.

Study approval

All human studies were conducted with the approval of the Seattle Children's and Fred Hutch Cancer Center Institutional Review Boards. The reanalysis of publicly available single cell RNA sequencing data (20) used only deidentified data and does not meet the

definition of human subjects research. All mouse studies were approved by the Seattle Children's Research Institute Animal Use and Care Committee.

Data availability

All original data will be made available by the authors upon reasonable request. Values for all data points in graphs are reported in the Supporting Data Values file.

Author Contributions

LP, YTT, HKL, LF, HG, AS and JG conceived and designed the study. AH, CJT, CA, and RAG conducted the clinical trials that provided patient serum samples for analysis. KB and HG analyzed patient samples. LP, YTT, HKL, LF, KB, MB, EF, HG and JG analyzed the data. LP, YTT, HKL, LF, MB and JG performed the in vivo and in vitro experiments. LP and JG wrote the original draft of the manuscript. LP, YTT, HKL, CJT, RAG, HG and JG revised the manuscript. All authors reviewed and approved the manuscript.

Conflicts of Interest

CJT received research funding from Juno Therapeutics/BMS, Nektar Therapeutics, 10X Genomics, and Genscript. CJT serves ad hoc advisory/consultant roles at Prescient Therapeutics, Century Therapeutics, Boxer Capital, Novartis, Merck Sharp and Dohme, and Abbvie. CJT is an inventor on patents related to CAR T-cell therapy. LP, YTT, HKL, LF, KB, EF, MB, AS, AH, CA, RAG, HG and JG declare no conflicts of interest.

Acknowledgments

This work was supported by the National Institutes of Health K08NS118138 (JG), R37CA275954 (JG), R37CA26677 (HHG), P30CA015704 (HHG); American Cancer Society/St. Baldrick's Foundation 933283 (HHG); and the Norcliffe Foundation Center for Integrative Brain Research at Seattle Children's Research Institute (JG).

References

1. Gust J, Taraseviciute A, Turtle CJ. Neurotoxicity Associated with CD19-Targeted CAR-T Cell Therapies. *CNS Drugs*. 2018;32(12):1091-1101. doi:10.1007/s40263-018-0582-9

2. Lee DW, et al. ASTCT Consensus Grading for Cytokine Release Syndrome and Neurologic Toxicity Associated with Immune Effector Cells. *Biol Blood Marrow Transplant J Am Soc Blood Marrow Transplant*. 2019;25(4):625-638. doi:10.1016/j.bbmt.2018.12.758

3. Gust J, et al. Glial injury in neurotoxicity after pediatric CD19-directed chimeric antigen receptor T cell therapy. *Ann Neurol*. 2019;86(1):42-54. doi:10.1002/ana.25502

4. Faulhaber LD, et al. Brain capillary obstruction during neurotoxicity in a mouse model of anti-CD19 chimeric antigen receptor T-cell therapy. *Brain Commun*. 2022;4(1):fcab309. doi:10.1093/braincomms/fcab309

5. Engelhardt B, Ransohoff RM. Capture, crawl, cross: the T cell code to breach the blood–brain barriers. *Trends Immunol*. 2012;33(12):579-589. doi:10.1016/j.it.2012.07.004

6. Gust J, et al. Cytokines in CAR T Cell–Associated Neurotoxicity. *Front Immunol*. 2020;11. doi:10.3389/fimmu.2020.577027

7. Hogg N, Patzak I, Willenbrock F. The insider's guide to leukocyte integrin signalling and function. *Nat Rev Immunol*. 2011;11(6):416-426. doi:10.1038/nri2986

8. Wong D, Dorovini-Zis K. Expression of vascular cell adhesion molecule-1 (VCAM-1) by human brain microvessel endothelial cells in primary culture. *Microvasc Res*. 1995;49(3):325-339. doi:10.1006/mvre.1995.1028

9. Gust J, et al. Endothelial Activation and Blood-Brain Barrier Disruption in Neurotoxicity after Adoptive Immunotherapy with CD19 CAR-T Cells. *Cancer Discov*. 2017;7(12):1404-1419. doi:10.1158/2159-8290.CD-17-0698

10. Gust J, et al. Glial injury in neurotoxicity after pediatric CD19-directed CAR-T cell therapy. *Ann Neurol*. Published online 2019.

11. Kochenderfer JN, et al. Long-Duration Complete Remissions of Diffuse Large B Cell Lymphoma after Anti-CD19 Chimeric Antigen Receptor T Cell Therapy. *Mol Ther J Am Soc Gene Ther*. 2017;25(10):2245-2253. doi:10.1016/j.ymthe.2017.07.004

12. Santomasso BD, et al. Clinical and Biological Correlates of Neurotoxicity Associated with CAR T-cell Therapy in Patients with B-cell Acute Lymphoblastic

Leukemia. *Cancer Discov*. 2018;8(8):958-971. doi:10.1158/2159-8290.CD-17-1319

13. Teachey DT, et al. Identification of Predictive Biomarkers for Cytokine Release Syndrome after Chimeric Antigen Receptor T cell Therapy for Acute Lymphoblastic Leukemia. *Cancer Discov*. 2016;6(6):664-679. doi:10.1158/2159-8290.CD-16-0040

14. Bender DE, et al. Cytokine Profiling in Plasma from Patients with Brain Tumors Versus Healthy Individuals using 2 Different Multiplex Immunoassay Platforms. *Biomark Insights*. 2021;16:11772719211006666. doi:10.1177/11772719211006666

15. Kim HO, et al. Serum cytokine profiles in healthy young and elderly population assessed using multiplexed bead-based immunoassays. *J Transl Med*. 2011;9(1):113. doi:10.1186/1479-5876-9-113

16. Yan F, et al. Potential role between inflammatory cytokines and Tie-2 receptor levels and clinical symptoms in patients with first-episode schizophrenia. *BMC Psychiatry*. 2023;23:538. doi:10.1186/s12888-023-04913-7

17. Steinman L. Blocking adhesion molecules as therapy for multiple sclerosis: natalizumab. *Nat Rev Drug Discov*. 2005;4(6):510-518. doi:10.1038/nrd1752

18. Turtle CJ, et al. Durable Molecular Remissions in Chronic Lymphocytic Leukemia Treated With CD19-Specific Chimeric Antigen Receptor–Modified T Cells After Failure of Ibrutinib. *J Clin Oncol*. 2017;35(26):3010-3020. doi:10.1200/JCO.2017.72.8519

19. Gardner RA, et al. Intent to treat leukemia remission by CD19CAR T cells of defined formulation and dose in children and young adults. *Blood*. Published online

January 1, 2017:blood-2017-02-769208. doi:10.1182/blood-2017-02-769208

20. Haradhvala NJ, et al. Distinct cellular dynamics associated with response to CAR-T therapy for refractory B cell lymphoma. *Nat Med*. 2022;28(9):1848-1859. doi:10.1038/s41591-022-01959-0

21. Jeong HW, et al. Single-cell transcriptomics reveals functionally specialized vascular endothelium in brain. Bautch VL, Rothlin CV, eds. *eLife*. 2022;11:e57520. doi:10.7554/eLife.57520

22. Vinnakota JM, et al. Targeting TGFβ-activated kinase-1 activation in microglia reduces CAR T immune effector cell-associated neurotoxicity syndrome. *Nat Cancer*. 2024;5(8):1227-1249. doi:10.1038/s43018-024-00764-7

23. Cruz Hernández JC, et al. Neutrophil adhesion in brain capillaries reduces cortical blood flow and impairs memory function in Alzheimer's disease mouse models. *Nat Neurosci*. 2019;22(3):413-420. doi:10.1038/s41593-018-0329-4

24. Amki ME, et al. Neutrophils Obstructing Brain Capillaries Are a Major Cause of No-Reflow in Ischemic Stroke. *Cell Rep*. 2020;33(2). doi:10.1016/j.celrep.2020.108260

25. Lim HK, et al. Seizure-induced neutrophil adhesion in brain capillaries leads to a decrease in postictal cerebral blood flow. *iScience*. 2023;26(5):106655. doi:10.1016/j.isci.2023.106655

26. Iadecola C, et al. Immune responses to stroke: mechanisms, modulation, and therapeutic potential. *J Clin Invest*. 2020;130(6):2777-2788. doi:10.1172/JCI135530

27. Norelli M, et al. Monocyte-derived IL-1 and IL-6 are differentially required for cytokine-release syndrome and neurotoxicity due to CAR T cells. *Nat Med*. 2018;24(6):739-748. doi:10.1038/s41591-018-0036-4

28. Wang H, et al. Triple knockdown of CD11a, CD49d, and PSGL1 in T cells reduces CAR-T cell toxicity but preserves activity against solid tumors in mice. *Sci Transl Med*. 2025;17(782):eadl6432. doi:10.1126/scitranslmed.adl6432

29. Davila ML, et al. CD19 CAR-targeted T cells induce long-term remission and B Cell Aplasia in an immunocompetent mouse model of B cell acute lymphoblastic leukemia. *PloS One*. 2013;8(4):e61338. doi:10.1371/journal.pone.0061338

30. Li G, et al. Gammaretroviral Production and T Cell Transduction to Genetically Retarget Primary T Cells Against Cancer. *Methods Mol Biol Clifton NJ*. 2017;1514:111-118. doi:10.1007/978-1-4939-6548-9_9

31. Shih AY, et al. A Polished and Reinforced Thinned-skull Window for Long-term Imaging of the Mouse Brain. *J Vis Exp JoVE*. 2012;(61). doi:10.3791/3742

32. Shih AY, et al. Two-photon microscopy as a tool to study blood flow and neurovascular coupling in the rodent brain. *J Cereb Blood Flow Metab*. 2012;32(7):1277-1309. doi:10.1038/jcbfm.2011.196

33. Dimitrov S, et al. Activated integrins identify functional antigen-specific CD8+ T cells within minutes after antigen stimulation. *Proc Natl Acad Sci*. 2018;115(24):E5536-E5545. doi:10.1073/pnas.1720714115

34. Turtle CJ, et al. CD19 CAR–T cells of defined CD4+:CD8+ composition in adult B

cell ALL patients. *J Clin Invest*. 2016;126(6):2123-2138. doi:10.1172/JCI85309

Figure 1

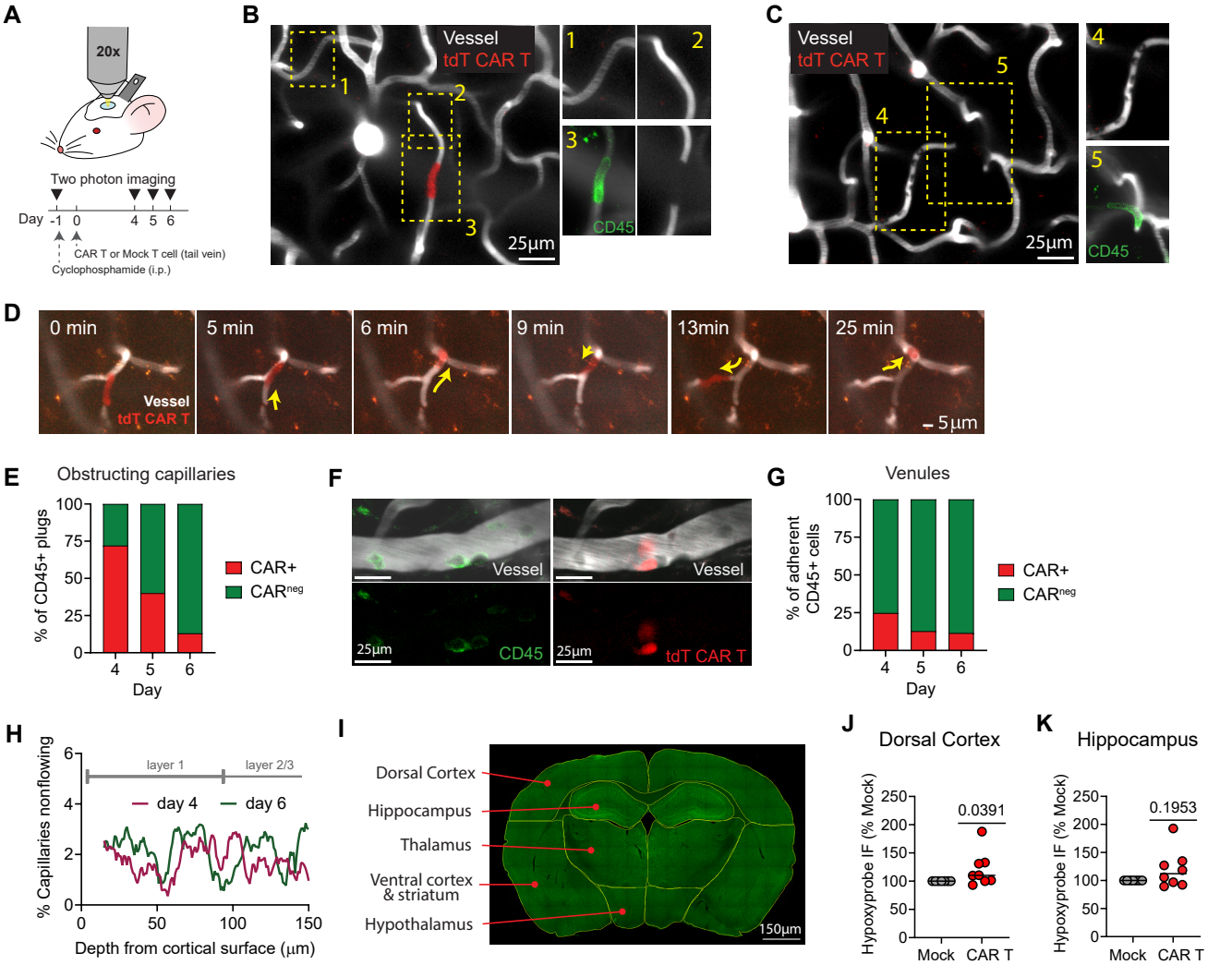

Figure 1. CAR T cells obstruct blood flow in brain capillaries during CD19-CAR T neurotoxicity.
(A) Schematic of in vivo two photon imaging through a cranial window. **(B)** CAR T cell (red) obstructing a brain capillary, seen as top-down view through the cranial window. Insets: 1, example of a flowing capillary, with striations created by transiting red blood cells. 2, nonflowing capillary due to obstructing CAR T cell, note absence of striations. 3, colabeling of CAR T cell with intravascularly delivered anti-CD45 antibody (left), and flow void created by the CAR T cell (right). **(C)** example of a non-CAR T leukocyte obstructing a capillary. Insets: 4, flow voids created by stalled red blood cells behind the leukocyte. 5, CD-45 labeling to confirm the obstructing object is a leukocyte. **(D)** Example of a stalled CAR T cell (red) moving back and forth within the capillary network over the span of 25 minutes. **(E)** Bar graph showing the fraction of stalled CD45+ cells that were td-tomato positive CAR T cells, n=8 mice. **(F)** Representative example of adherent leukocytes in a pial venule. The left and right images were acquired serially within 2 minutes of each other, because different excitation wavelengths were required for optimal acquisition of the CD45-Alexa488 and the td-Tomato labels. Therefore, the cells have moved slightly between images. **(G)** Bar graph showing the cumulative proportion of td-Tomato positive CAR T cells among adherent cells in pial and dural venules, n=8 mice. **(H)** Percentage of stalled capillaries by depth from cortical surface. The lines show the running average (smoothened by 10 nearest neighbors on each side) of 1µm depth steps. The top 20µm is not shown to avoid edge artifact. **(I)** Coronal section of CAR T treated mouse brain stained for hypoxyprobe (green). The annotations show the regions that were manually segmented for analysis. **(J, K)** Scatter plots showing the mean brightness of hypoxyprobe immunofluorescence (IF) in the cortex and hippocampus. Values are normalized to mock treated control. Each dot indicates one mouse. One-sample Wilcoxon test with theoretical median set at 100, n=8. The mock control values (n=7) are all 100% and are only shown for reference.

Figure 2

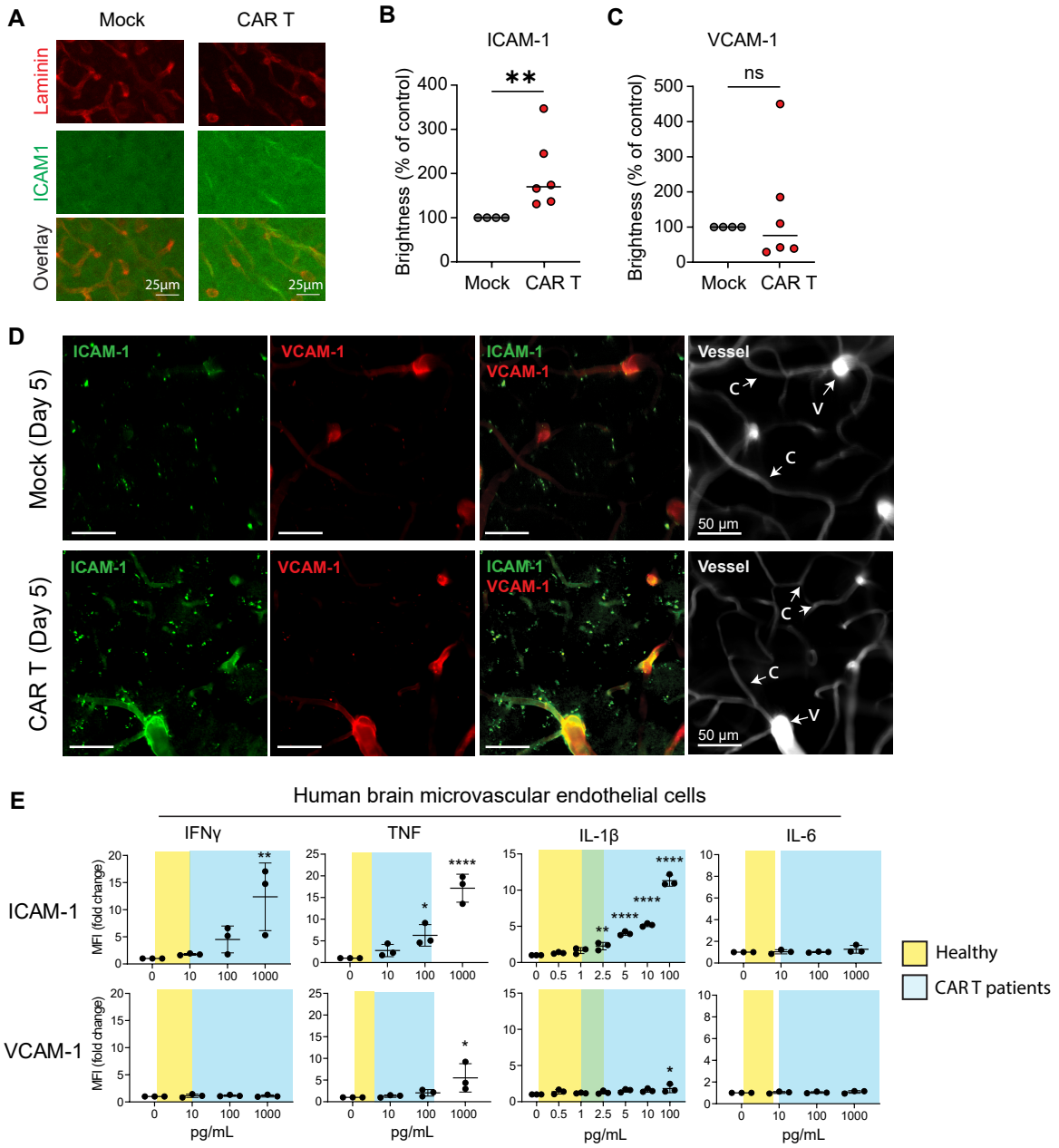

Figure 2. ICAM-1 is widely upregulated in brain capillaries in CD19-CAR T cell treated mice.
(A) Representative immunofluorescence images showing capillary labeling with anti-laminin antibody (neuronal nuclei are also labeled) and ICAM-1 staining. These images were analyzed to obtain the data in **B** and **C**, which show scatter plots of ICAM-1 and VCAM-1 immunofluorescence brightness, as normalized to mock control. Each dot indicates one mouse. One-sample Wilcoxon test with theoretical median set at 100, n=6. The mock control values (n=4) are all 100% and are only shown for reference. **(D)** Representative top down view of the cortical microvasculature by in vivo two-photon imaging. ICAM-1 and VCAM-1 were labeled with intravascular fluorescent antibodies in mice treated with mock (top row) or CAR T cells (bottom row). c, capillary; v, venule. **(E)** Scatter plots showing upregulation of ICAM-1 and VCAM-1 in hBMECs after treatment with cytokines. The y-axis indicates the fold change in mean fluorescence intensity as measured by flow cytometry, comparing each data point to the 0 pg/mL vehicle-only control within the same experiment. The x-axis indicates the concentration of each cytokine that was added to the culture media for 24h. The yellow shading indicates the approximate concentrations of each cytokine found in the blood of healthy volunteers, the blue shading indicates the range of concentrations reported in CAR T cell patients, and green shows overlap of these ranges. N=3 independent experiments, one-way ANOVA with Dunnett's multiple comparisons test, only comparisons with the 0 pg/mL vehicle-only control were performed. *P<0.05, **P<0.01, ***P<0.001, ****P<0.0001. All others are P>0.05.

Figure 3

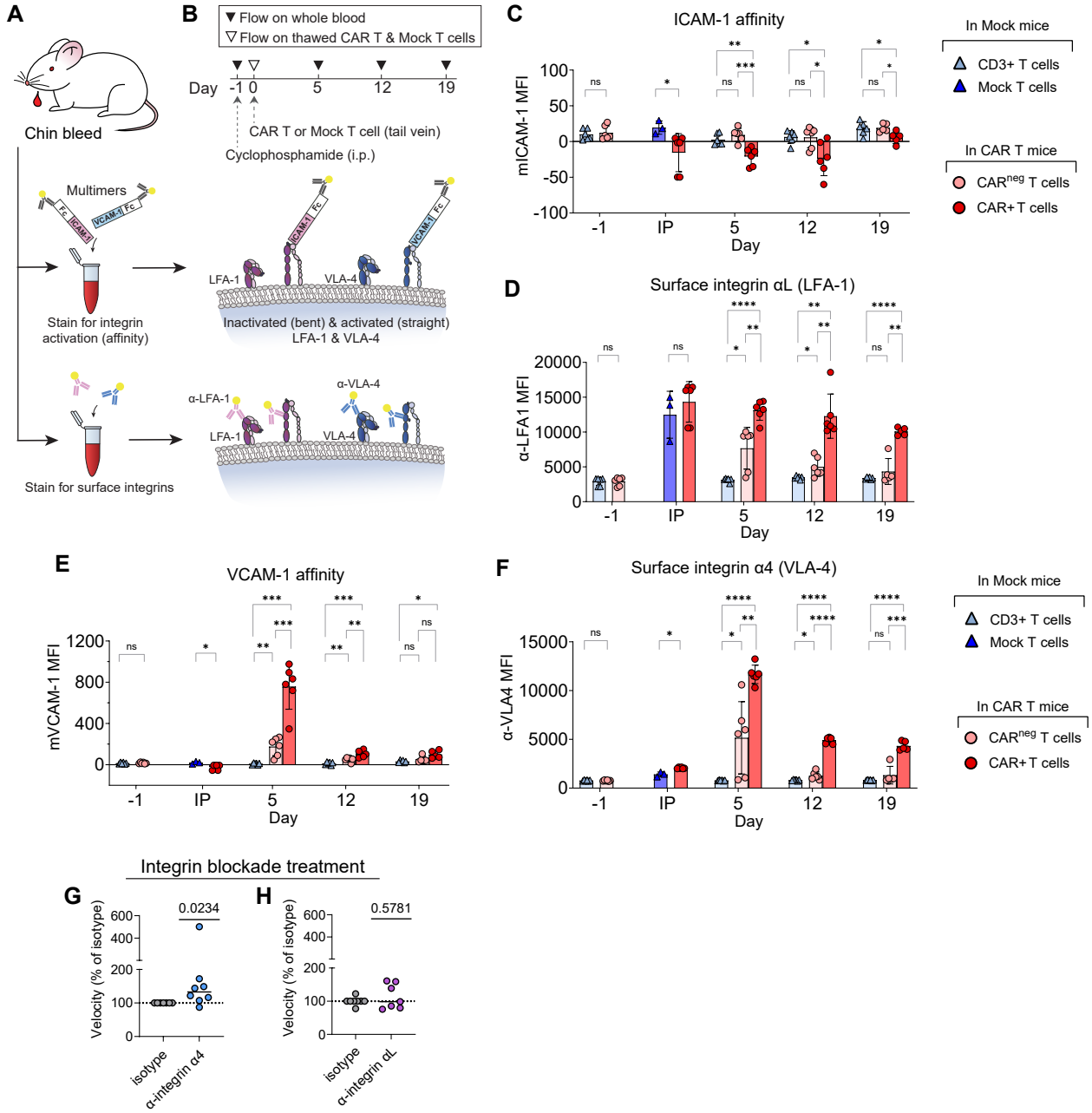

Figure 3. CAR T cells strongly upregulate affinity of VLA-4 to VCAM after infusion.
(A) Schematic of experimental design. **(B)** Timeline of experimental design. **(C-F)** Scatter plots showing flow cytometric measurements of T cell affinity to ICAM-1 **(C)**, surface expression of integrin αL (LFA-1, **D**), affinity to VCAM-1 **(E)**, and surface expression of integrin α4 (VLA-4, **F**). The y-axis indicates the mean fluorescence intensity (MFI, arbitrary units) for each analyte, and the x-axis indicates time relative to CAR T cell infusion, IP = cryopreserved infusion product. Measurements are compared between mice treated with mock transduced T cells (blue triangles) and mice treated with CD19-CAR T cells (red circles). Each data point indicates one mouse, the box plots show the mean and the whiskers show the standard deviation. N=3 independent experiments, for a total of 3-6 mice per group. All comparisons are by unpaired 2-sample t test with Welch correction, *P<0.05, **P<0.01, ***P<0.001, ****P<0.0001, ns P>0.05. **(G, H)** Scatter plots showing movement velocity in the open-field test after treatment with antibody to block function of integrin α4 **(G)** or integrin αL **(H)**. Values are normalized to mock treated control. Each dot indicates one mouse. Data is summarized from 3 or more independent experiments. Statistics are by one-sample Wilcoxon test with theoretical median set at 100, n=7-8. The mock control values (n=7-8) are only shown for reference.

Figure 4

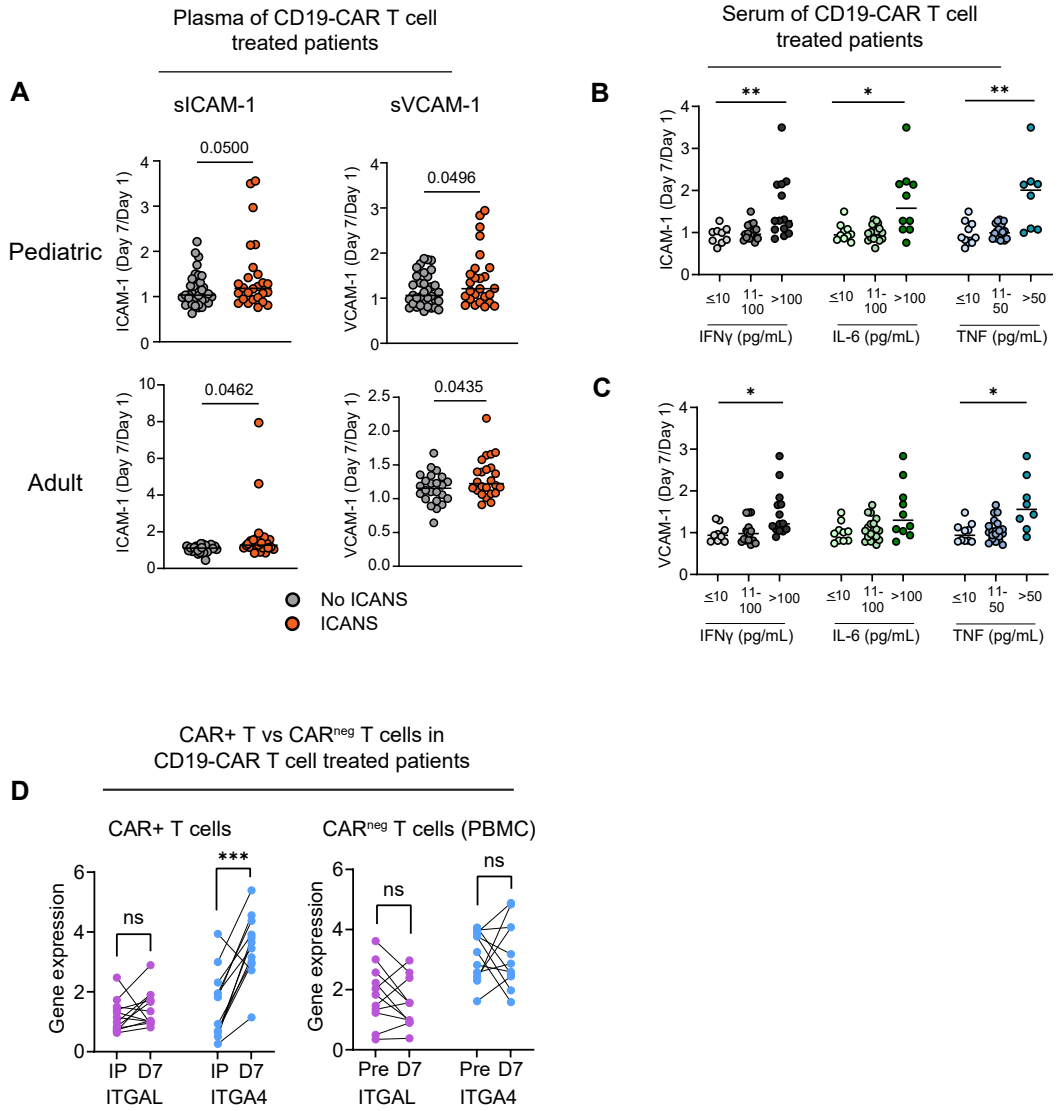

Figure 4. Endothelial-leukocyte adhesion molecule dynamics in CD19-CAR T cell patients.
(A) Scatter plots showing ratio of Day 7/Day 1 serum levels of soluble ICAM-1 or VCAM-1 in two independent clinical cohorts. The line indicates the mean, comparisons as by unpaired 2-sided t test. **(B,C)** Scatter plots showing Day 7/Day 1 serum levels of soluble ICAM-1 and VCAM-1 as they correlate with serum cytokine levels on day 7. Patients were grouped by cytokine levels analogous to the concentrations used in the in vitro experiments in Figure 2. The lines indicate the median, Kruskal-Wallis test with Dunn's multiple comparisons posttest, only comparisons with the <10pg/mL group were performed. *P<0.05, **P<0.01, all other comparisons are P>0.05. **(D)** Integrin gene expression levels in sorted CAR T cells or CAR-negative T cells by pseudobulk reanalysis of single cell RNA sequencing data. Each data point represents one sample, paired samples from individual patients are connected by lines. IP, infusion product; D7, PBMCs on day 7 after CAR T cell infusion; Pre, baseline PBMC sample prior to CAR T cell infusion. Paired 2-sided t test, *P<0.05, **P<0.01, ***P<0.001, ****P<0.0001, ns P>0.05.